Reaction-Limited Aggregation in Presence of Short-Range Structural Forces

Venkataramana Runkana
NSF Industry/University Cooperative Research Center for Advanced Studies in Novel Surfactants, School of Engineering and Applied Science, Columbia University, New York, NY 10027

Tata Research Development and Design Centre, 54-B, Hadapsar Industrial Estate, Pune, 411013 India

P. Somasundaran
NSF Industry/University Cooperative Research Center for Advanced Studies in Novel Surfactants, School of Engineering and Applied Science, Columbia University, New York, NY, 10027

P. C. Kapur
Tata Research Development and Design Centre, 54-B, Hadapsar Industrial Estate, Pune, 411013 India

DOI 10.1002/aic.10375
Published online March 3, 2004 in Wiley InterScience (www.interscience.wiley.com).

A geometrically discretized sectional population balance model for reaction-limited aggregation of colloidal suspensions is presented. The two important model parameters are collision frequency factor and collision efficiency factor. The collision frequency factor is derived from physically realistic arguments proposed for collision of fractal aggregates. The collision efficiency factor is computed as a function of total interaction energy between particles, including short-range structural repulsion forces. The irregular and open structure of aggregates is taken into account by incorporating their mass fractal dimension. The characteristic time constant of reaction-limited aggregation, derived from dynamic scaling of mean aggregate size-aggregation time data, is found to correlate with electrolyte concentration. The population balance model is tested with published experimental data for aggregation of γ-alumina suspensions in the presence of different electrolytes. It is shown that the slow kinetics of aggregation under certain conditions of pH and electrolyte concentration require inclusion of short-range structural repulsion forces along with van der Waals attraction and electrical double layer repulsion forces in an extended DLVO theory. The model predictions are in good agreement with experimental data for time evolution of mean aggregate diameter in the reaction-limited aggregation regime. © 2005 American Institute of Chemical Engineers
AIChE J, 51: 1233–1245, 2005
Keywords: reaction-limited aggregation, population balance modeling, surface forces, fractal aggregates, colloidal suspensions

Introduction

Aggregation of colloidal suspensions plays an important role in treatment of municipal and industrial water, beneficiation of minerals, manufacture of pulp and paper, processing of paints and pharmaceuticals and in fabrication of ceramics[1, 2, 3, 4]. Transport and fate of contaminants in the aquatic environment depend to a large extent on aggregation of colloids in the presence of naturally occurring salts and polymers[5]. The aggregation phenomenon is usually classified in two regimes - diffusion-limited aggregation (DLA) and reaction-limited aggregation (RLA)[6]. DLA occurs when collision efficiency of

Correspondence concerning this article should be addressed to P. Somasundaran at ps24@columbia.edu

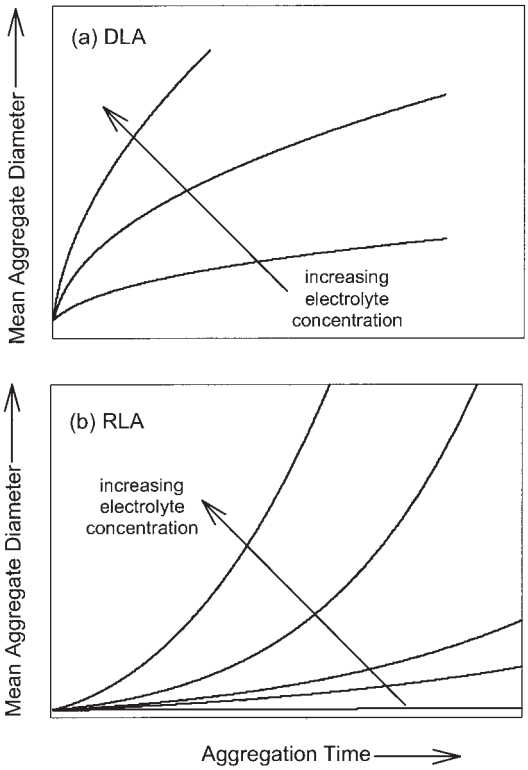

Figure 1 Representative aggregate growth curves (a) diffusion-limited aggregation - power law growth, and (b) reaction-limited aggregation - exponential growth.

two clusters is relatively high or close to unity, while RLA prevails at very low collision efficiencies. Because of differences in hydrodynamics of particle/cluster interactions, the kinetics of aggregation are dissimilar in the two regimes. DLA follows power-law growth kinetics (Figure 1a) while RLA kinetics conforms to an exponential growth law (Figure 1b).

Starting with the classical work of Smoluchowski[7], particle population balance has been widely employed to model aggregation of colloidal suspensions and evolution of aggregate size distribution in time. The two important model parameters in the population balance equation (PBE) are collision frequency factor or collision kernel and collision efficiency factor. It is known that DLA kinetics by Brownian motion is well represented by the Smoluchowski kernel[7]. Although several expressions, both empirical and theoretical, have been proposed, there is as yet no general agreement on an appropriate kernel for RLA kinetics. Recently, Sandkuhler et al.[8] evaluated a number of kernels and concluded that even though none could represent the experimental data accurately, the product kernel or its modification by Odriozola et al.[9] is the most appropriate for the process. Other authors have concluded that RLA kinetics are best described by a sum kernel[10, 11]. In fact, the earlier experimental studies on aggregation of polystyrene[12] and gold colloids[13] had shown that RLA kinetics could be represented reasonably well by an empirical sum kernel.

The second parameter in the PBE is collision efficiency factor. Except in a few instances[14, 15], this is either assumed to be unity or treated as a floating parameter for fitting experimental aggregate size distribution data. The collision efficiency is a function of the interaction forces between suspended particles and aggregates or clusters, which may include van der Waals or dispersion attraction, electrical double layer (EDL) repulsion and short-range structural repulsion forces. Despite its known limitations, the classical DLVO theory[16, 17] is quite successful in accounting for the role of dispersion and EDL forces in the stability of colloids in the presence of inorganic electrolytes. However, under certain conditions of pH and salt concentration, an additional repulsive force, generally termed as structural or hydration force, has been observed between several materials at short separation distances ($<$ 3–5 nm)[18, 19, 20, 21]. This short-range hydration repulsion is thought to play an important role in the fabrication of ceramic components[22] and in the stability of latex immunoassays[23]. More pertinently, there now exists considerable evidence which suggests that the short-range structural forces can modify the kinetics of aggregation, as elaborated in the following paragraph.

Recently, Waite and coworkers[24, 25] and van Bruggen et al.[26] studied the stability and aggregation behavior of several aluminum oxide suspensions in the presence of different salts. Beattie et al.[24] examined aggregation of suspensions of γ-alumina (γ-Al_2O_3), boehmite (γ-AlOOH, aluminum oxide hydroxide or alumina monohydrate) and gibbsite (γ-$Al(OH)_3$, aluminum trihydroxide or alumina trihydrate). They concluded that the stability of gibbsite suspensions was similar to that of oxides, such as hematite, and the critical coagulation concentration was close to 50 mM NaCl in pH range 5-6. The other aluminum oxides, however, exhibited somewhat anomalous behavior. In neutral pH conditions the suspensions coagulated at low salt concentrations, while at lower pH levels coagulation took place only at much higher salt concentrations. At a pH of 4.5, aggregation of γ-alumina was observed only above 0.5 M KCl concentrations, and of boehmite at 0.13 M and above. Waite et al.[25] reported similar results for γ-alumina in the presence of NaCl and KNO_3, that is, aggregation was observed at salt concentrations above 0.5 M only. This behavior was attributed to the adsorption of aluminum tridecamer, $Al_{13}O_4(OH)_{24}(H_2O)_{12}^{7+}$ on alumina surface. In addition to the aggregation studies, force measurements by atomic force microscopy[21] between an aluminum-coated silica sphere and a flat aluminum substrate have shown the existence of short-range ($<$ 3 nm) repulsive forces in 1 mM KCl at different pH levels. At high pH, the short-range repulsion was attributed to the swelling of sapphire surface and formation of a thick, approximately 15 nm, hydrated gel layer adjacent to the alumina surface. No swelling was observed at low pH and repulsion was assumed to be due to hydration. The DLVO type forces could explain the interaction only up to surface separation distance of about 3 – 5 nm. In order to describe the force-distance profiles at shorter separations, it was necessary to invoke an additional repulsive force. Similar short-range forces were also observed between sapphire surfaces in 0.1 M NaBr solutions at pH 3[20].

Interestingly, in the studies of Beattie et al.[24] and Waite et al.[25], aggregation kinetics followed an exponential growth, suggesting that the phenomenon took place under RLA conditions, presumably due to low efficiency of the particle/aggregate collisions. Although it is not clear whether adsorption of aluminum tridecamer or any other polymeric species on particle surface or hydration of the surface was responsible for the

anomalous aggregation behavior, it seems very likely that repulsive forces, other than the classical DLVO forces, were in operation in the aforementioned experiments.

The objective of this work is to develop a population balance model for aggregation processes that follow the slow exponential growth kinetics. Toward this end, we employ a geometrically sectioned discrete population balance equation for aggregation. The collision kernel in the model is based on theoretical arguments advanced by Ball et al.[1], and the collision efficiency factor is computed as a function of interaction forces between particles including the short-range structural forces. The model is tested and verified with experimental data for slow aggregation of alumina suspensions in the presence of different salts as reported by Beattie et al.[24] and more recently by Waite et al.[25].

Model of Reaction-Limited Aggregation Kinetics

Population balance equation (PBE)

The evolution of floc or aggregate size distribution in time, which is the focus of this study, can be simulated within the framework of particle population balance. The size-continuous form of population balance equation for aggregation in a spatially homogeneous batch process is given by[7]

$$\frac{\partial n(v,t)}{\partial t} = -\int_0^\infty \alpha(v,u)\beta(v,u)n(v,t)n(u,t)du + \frac{1}{2}\int_0^v \alpha(v-u,u)\beta(v-u,u)n(v-u,t)n(u,t)du \quad (1)$$

where n is number concentration of aggregates (or particles), v and u denote aggregate volume, t is aggregation time, β is collision frequency factor and α is collision efficiency factor. The first term on right-hand side accounts for the loss or disappearance of aggregates of size v due to their interaction with aggregates of all sizes. The second term represents the rate of formation of aggregates of size v by interaction between two aggregates of smaller sizes. This partial integrodifferential equation does not admit of close form analytical solutions unless drastically simplified and generally unrealistic collision kernels are employed. Consequently, the aggregation equation is invariably solved numerically after discretizing and lumping it into a set of nonlinear ordinary differential equations. Of the several discretization and lumping schemes available in the literature[27, 28], we have chosen the method of geometric sections proposed by Hounslow et al.[29] because it is computationally less intensive and easy to implement. The rate of change of particle or floc concentration due to aggregation alone, that is, for processes that do not involve fragmentation of flocs, is given by[29]

$$\frac{dN_i}{dt} = N_{i-1}\sum_{j=1}^{i-2} 2^{j-i+1}\alpha_{i-1,j}\beta_{i-1,j}N_j + \frac{1}{2}\alpha_{i-1,i-1}\beta_{i-1,i-1}N_{i-1}^2 - N_i\sum_{j=1}^{i-1} 2^{j-i}\alpha_{i,j}\beta_{i,j}N_j - N_i\sum_{j=i}^{max}\alpha_{i,j}\beta_{i,j}N_j \quad (2)$$

where N_i is number concentration of particles or aggregates in section i. The first term on right-hand side accounts for growth due to aggregation of clusters belonging to all the smaller sections, except the immediately adjacent smaller one. The second term represents growth due to aggregation of clusters belonging to the section immediately smaller than section i. The third term accounts for loss of aggregates due to their interaction with those belonging to all the smaller sections, and the fourth term represents loss of aggregates due to mutual aggregation, and due to their interactions with larger aggregates belonging to higher sections. The smallest section corresponds to primary particles and *max* is the section that contains aggregates with the largest characteristic volume. The frequency of collisions is directly related to collision volume of the aggregates. The characteristic volume V_i of an aggregate in section i is computed as the arithmetic mean of its lower and upper bounds[30]

$$V_i = \frac{b_i + b_{i-1}}{2} \quad (3)$$

where b_{i-1} and b_i are the smallest and the largest volumes in section i, respectively. Moreover, the upper bound is computed as a function of the lower one with a geometric sectional spacing factor of 2

$$b_i = 2b_{i-1} \quad (4)$$

The primary particle volume is denoted by V_1. An aggregate of volume V_i comprises 2^{i-1} primary particles. The rate of aggregation depends on particle concentration and frequency and efficiency of particle/aggregate collisions. The frequency of collisions is governed by suspension hydrodynamics and, in addition, depends on a number of factors such as particle/aggregate size, temperature and solvent viscosity. The efficiency of collisions, on the other hand, depends critically on surface and colloid chemistry of the suspension. It is a function of pH, electrolyte concentration and electrochemical nature of particle surface, besides the variables mentioned previously.

Collision Kernel

In case of DLA, particles are expected to aggregate in the first instance of collision only. Hence, the collision frequency is directly related to collision cross-section and particle diffusion coefficient. In case of RLA, however, it is generally believed that repeated collisions are required for a successful event of aggregation. Accordingly, the aggregates involved in the collision process sample several sites on each other's surface before attachment actually occurs. Unlike the collision kernel for DLA, which was derived by Smoluchowski[7] on theoretical considerations quite some time ago, a rigorous expression does not exist for the RLA kernel. Instead of using an *ad hoc* empirical kernel, we have applied the theoretical arguments of Ball et al.[1] to compute the collision frequency factor. These authors considered two regimes of aggregate collisions: first, collisions between clusters of approximately equal masses, and second, collisions between large clusters and very small clusters. It was assumed that these two regimes are sufficient to describe the aggregation rate. Moreover, they

concluded on basis of theoretical scaling arguments that the cluster sizes are determined mainly by collisions involving large and small clusters rather than those involving clusters of equal masses. However, Sandkuhler et al.[8] recently concluded that a kernel, derived from such scaling arguments, which is essentially a function of mass of the larger of the two interacting clusters, is not accurate enough for reaction-limited aggregation. This is not surprising since the final aggregate mass distribution depends strongly on interactions involving clusters of all sizes rather than those involving very small and very large clusters only. We therefore modify the treatment of Ball et al.[1] in order to account for masses or sizes of both interacting clusters.

Ball et al.[1] proposed that the rate coefficient for RLA is directly proportional to the volume of phase-space V_f, over which the center of one cluster can be positioned such that the two clusters are in bondable contact. Two clusters are assumed to be in bondable contact if they are within a microscopic distance h_w, of touching each other, but not overlapping. This distance can be of the order of the repulsive barrier between two colliding particles and is significantly less than the cluster size. For small h_w, V_f is directly proportional to the contact surface of two interacting aggregates. For two solid spheres of radii r_1 and r_2, the volume of phase-space is given by[1]

$$V_f = 4\pi(r_1 + r_2)^2 h_w \; ; \; h_w \ll r_1, \; r_2 \tag{5}$$

For two fractal aggregates i and j with collision radii r_{c_i} and r_{c_j} respectively, the collision frequency is then given by

$$\beta_{i,j} \propto (r_{ci} + r_{cj})^2 \tag{6}$$

The above equation can be rewritten as follows

$$\beta_{i,j} = K_{RLA}(r_{ci} + r_{cj})^2 \tag{7}$$

where K_{RLA} is a proportionality constant or lumped parameter, which takes into account the effect of temperature and viscosity of the suspension, besides the parameter h_w. The collision radius of an aggregate containing n_0 monodisperse primary particles of radius r_0 is given by[31]

$$r_{ci} = r_0\left(\frac{n_{0i}}{C_L}\right)^{1/d_F} \tag{8}$$

where d_F and C_L are aggregate fractal dimension and structure prefactor, respectively. Experimental studies on aggregation of latex suspensions indicate that C_L is of the order one[32, 33]. Finally, substituting Eq. 8 into Eq. 7 yields the following expression for the RLA collision kernel

$$\beta_{i,j} = K_{RLA} r_0^2\left(\frac{1}{C_L}\right)^{2/d_F}(n_{0_i}^{1/d_F} + n_{0_j}^{1/d_F})^2 \tag{9}$$

This equation is substituted into the PBE in Eq. 2 for simulating the RLA kinetics.

Collision efficiency

The probability of attachment, when two aggregates collide, depends mainly on the interaction between primary particles in the colliding surfaces rather than on particles residing in the interior. This is because forces between particles drop rapidly with distance and, as such, interaction between aggregates can be approximated by interaction between the primary surface particles[34, 35]. We take explicit cognizance of this fact by incorporating in our PBE a collision efficiency factor for aggregates which is computed as reciprocal of the modified Fuchs' stability ratio W between two primary particles k and l[36, 37, 38, 39]

$$W_{k,l} = \frac{\displaystyle\int_{r_{0_k}+r_{0_l}}^{\infty} D_{k,l}\frac{\exp(V_T/k_BT)}{s^2}\,ds}{\displaystyle\int_{r_{0_k}+r_{0_l}}^{\infty} D_{k,l}\frac{\exp(V_{vdW}/k_BT)}{s^2}\,ds} \tag{10}$$

where $D_{k,l}$ is hydrodynamic correction factor, given by[40]

$$D_{k,l} = \frac{6\bar{h}_0^2 + 13\bar{h}_0 + 2}{6\bar{h}_0^2 + 4\bar{h}_0} \tag{11}$$

and V_T is total energy of interaction, V_{vdW} is van der Waals energy of attraction between two primary particles of radii r_{0_k} and r_{0_l} (assumed spherical), $s = r_{0_k} + r_{0_l} + h_0$ is distance between particle centers, h_0 is distance of closest approach between particle surfaces and $\bar{h}_0 = 2h_0/(r_{0_k} + r_{0_l})$. Note that the influence of hydrodynamic forces at very short separation distances is accounted for in Eq. 10 by including the correction factor in Eq. 11.

Since our focus is on aggregation processes in which short-range structural forces play an important role, the classical DLVO theory is extended by incorporating short-range structural repulsion forces with van der Waals attraction and electrical double layer repulsion in the total energy of interaction between particles. The expressions employed for these forces are summarized below.

Interaction forces

The van der Waals energy of attraction between particles may be computed from either the Hamaker microscopic theory[41] or the Lifshitz macroscopic theory[42]. The relative merits of these theories are discussed elsewhere[43]. The latter is more rigorous than the former but requires accurate dielectric data for the materials involved. Because it is easier to implement, we have employed the Hamaker theory to compute the van der Waals energy of attraction V_{vdw} between a pair of spherical particles[41]

$$V_{vdW} = -\frac{A}{6}\left\{\frac{2r_{0_k}r_{0_l}}{s^2-(r_{0_k}+r_{0_l})^2}+\frac{2r_{0_k}r_{0_l}}{s^2-(r_{0_k}-r_{0_l})^2} + \ln\left[\frac{s^2-(r_{0_k}+r_{0_l})^2}{s^2-(r_{0_k}-r_{0_l})^2}\right]\right\} \quad (12)$$

where A is Hamaker constant of solids across the solvent medium. This expression does not take into account the retardation phenomenon, which sets in at about 5 nm from the particle surface[44]. The retardation effect is incorporated by multiplying the unretarded van der Waals force with a correction function f_R proposed by Gregory[45]

$$f_R(h_0) = 1 - \frac{g_R h_0}{\lambda_R}\ln\left(1+\frac{\lambda_R}{g_R h_0}\right) \quad (13)$$

where λ_R is characteristic wavelength of interaction and g_R is a fitting parameter. The value of λ_R is typically 100 nm and that of g_R is 5.32[45].

The main reason for the slow kinetics in RLA regime is the low collision efficiency. In other words, the repulsive forces are greater in magnitude than the attractive forces although not large enough to prevent aggregation completely. One of these forces arises from the interaction between electrical double layers (EDL), which exist at the solid-solution interface. When two particles of same material approach each other, they are subjected to electrostatic repulsion whose magnitude depends on surface charge density which, in turn, is a function of solution pH, temperature, and type and concentration of electrolyte species. The EDL interaction between particles can be treated rigorously by the nonlinear Poisson-Boltzmann equation. The solution of this equation is, however, a complex task, which is why several approximations based on linearization of the Poisson-Boltzmann equation have been proposed[46, 47, 48]. We have used the analytical expression proposed by Bell et al.[47], which is given by following expression for two spherical particles of radii r_{0_k} and r_{0_l} and surface potentials ψ_{0_k} and ψ_{0_l}

$$V_{edl} = 64\pi\varepsilon_r\varepsilon_0\left(\frac{k_BT}{z_ce}\right)^2\left(\frac{r_{0_k}r_{0_l}}{r_{0_k}+r_{0_l}}\right)\tanh\left(\frac{z_ce\psi_{0_k}}{4k_BT}\right) \times tanh\left(\frac{z_ce\psi_{0_l}}{4k_BT}\right)\exp(-\kappa h_0) \quad (14)$$

where e is elementary charge and z_c is valence of the counterion and ε_0 and ε_r are dielectric constants of a vacuum and solvent, respectively. The Debye-Huckel parameter κ is a function of temperature T, ionic strength I and dielectric constant ε_r of solution. It is computed in the usual manner[44]

$$\kappa = \left(\frac{2N_{Av}Ie^2}{\varepsilon_0\varepsilon_r k_BT}\right)^{1/2} \quad (15)$$

where N_{Av} is Avagadro's number and I is ionic strength of the solution, which is a function of electrolyte concentration and valence of electrolyte ions.

In addition to the EDL force, short-range repulsion also contributes to the low collision efficiency under certain conditions of pH and electrolyte concentration. Force measurements between surfaces of several materials, such as mica, silica and alumina have shown the existence of this force[18, 19, 20, 21]. It supposedly arises due to the structure of water or solvent molecules at the solid-liquid interface and is termed as hydration or solvation repulsion or more generally structural force. A number of theories have been proposed for this force but these have not been able to explain various experimental observations under different conditions[49, 50]. In the absence of a definitive theoretical expression, the following simple exponential decay function is deemed adequate for representing the experimental force-distance profiles[20, 44]

$$F_{hyd} = P_{hyd}\exp(-h_0/\lambda_{hyd}) \quad (16)$$

where P_{hyd} is termed structural or hydration force constant and λ_{hyd} is called hydration decay length. Their values have been found to be in the ranges of $10^6 - 5\times10^8$ N/m^2 and 0.2 – 1.0 nm, respectively[51]. The equation for hydration interaction energy between two spherical particles can be readily derived from Eq. 16, by applying the Derjaguin approximation[52], which for two unequal spherical particles of radii r_{0_k} and r_{0_i} is given by

$$V_{hyd} = \left(\frac{2\pi r_{0_k}r_{0_l}}{r_{0_k}+r_{0_l}}\right)P_{hyd}\lambda_{hyd}^2\exp(-h_0/\lambda_{hyd}) \quad (17)$$

where V_{hyd} is short-range hydration or structural interaction energy.

Model Implementation

Aggregation data

The population balance model was implemented and validated against published data[24, 25] for aggregation of γ-alumina suspensions in the presence of different salts. Beattie et al.[24] conducted a series of experiments at different salt (KCl) concentrations and measured mean hydrodynamic diameter of aggregates as a function of time by photon correlation spectroscopy (PCS). Waite et al.[25] also studied aggregation of γ-alumina using NaCl and KNO_3 electrolytes. The details of experimental procedures and results can be found in the cited references. Here we limit ourselves to summarizing the experimental conditions for the data used in model simulations. The mean radius of primary particles r_O was 60 nm and solids concentration in suspension was 12.5 g/L. This corresponds to a primary particle number concentration of approximately 4.32×10^{18} m^{-3}. The experiments were conducted at pH 4.5 in solutions of NaCl, KCl and KNO_3, at different salt concentrations while maintaining temperature at 25 $\pm$ 1 °C. The measured zeta potential of alumina particles was approximately 30 mV at pH 4.5 in KNO_3 solutions.

Dynamic scaling

It is well known that cluster or aggregate mass distributions exhibit dynamic scaling, irrespective of whether aggregation occurs in DLA or RLA regime[6, 13]. In former case, aggregate mass grows proportionately with time while it increases exponentially in the RLA regime. This characteristic behavior is

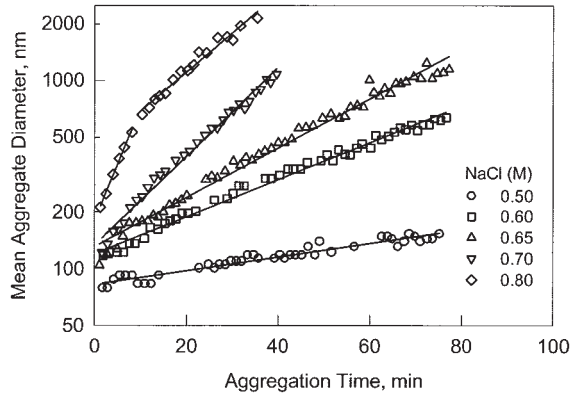

Figure 2 Semi-log plots for dynamic scaling of mean hydrodynamic diameter of γ-alumina aggregates in NaCl solutions at pH 4.5, showing exponential growth kinetics (data from Waite et al.[25]).

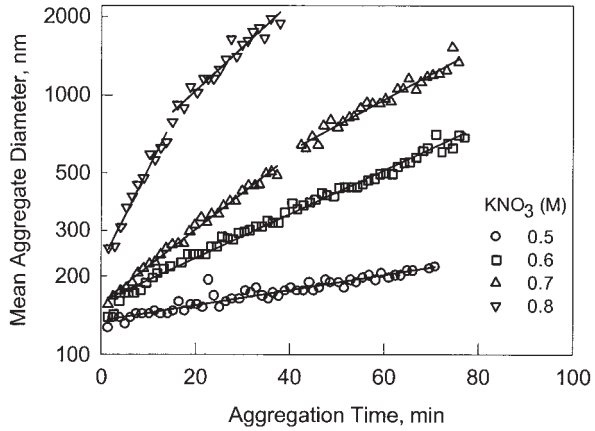

Figure 3 Semi-log plots for dynamic scaling of mean hydrodynamic diameter of γ-alumina aggregates in KNO_3 solutions at pH 4.5, showing exponential growth kinetics and shift in slope at high salt concentrations (data from Waite et al.[25]).

widely observed in a variety of particulate materials such as gold, silica and polystyrene latex[6, 53, 54]. We have utilized the principle of dynamic scaling to verify if aggregation of aluminum oxides took place under the universal slow RLA kinetics, wherein aggregate mass grows exponentially with time in following manner[6]

$$M \propto \exp\left(\frac{t}{\tau_{RLA}}\right) \tag{18}$$

where M is aggregate mass and τ_{RLA} is characteristic time constant of RLA, which depends on experimental conditions. If an aggregate is a fractal object and its mass scales with size, then the characteristic aggregate size r_n also has an exponential relationship with time

$$r_n \propto \exp\left(\frac{1}{\tau_{RLA} d_F}\, t\right) \tag{19}$$

Hence, a plot of mean aggregate size against time should be a straight line on a log-linear plot if aggregation follows the RLA kinetics. The experimental data of Beattie et al.[24] and Waite et al.[25] are plotted in Figures 2–4. It will be observed that γ-alumina aggregates exhibit dynamic scaling behavior at all times, and the aggregation phenomenon does follow the exponential growth kinetics provided salt concentrations are less than 0.8 M. The experimental data show a nonlinear relationship between aggregate size and time when salt concentrations are equal to or more than 0.8 M. It would seem that the process goes through a transition between RLA and DLA regimes as it approaches the fast DLA kinetics. However, in view of the fact that the plots are piece-wise linear, there is also a strong possibility of aggregate restructuring during aggregation. In this instance, how and when restructuring is triggered remains a question mark. Waite et al.[25] have also measured aggregate fractal dimensions and found them to be 2.09 and 2.1 at 0.6 M and 0.7 M NaCl, respectively. These values are similar to fractal dimensions observed for aggregates resulting by RLA[54, 55, 56]. A constant value of 2.1 for fractal dimension of all aggregates is employed in our analysis since it does not change with electrolyte concentration in the experimental studies of Waite et al.[25]. Substitutions of fractal dimension and slope of straight lines in Figures 2–4 in Eq. 19 yields an estimate of RLA time constant τ_{RLA}, which is plotted against salt concentration in Figure 5. It will be seen that τ_{RLA} decreases with salt content in a nonlinear fashion. This is an interesting result in the sense that above a critical concentration of 0.5 M the aggregation kinetics is controlled primarily by salt concentration. This behavior is similar to that normally observed in case of coagulation of colloidal suspensions. We are, therefore, obliged to conclude that there is a repulsive barrier, besides the electrical double layer force, that must be overcome in order for aggregation to take place.

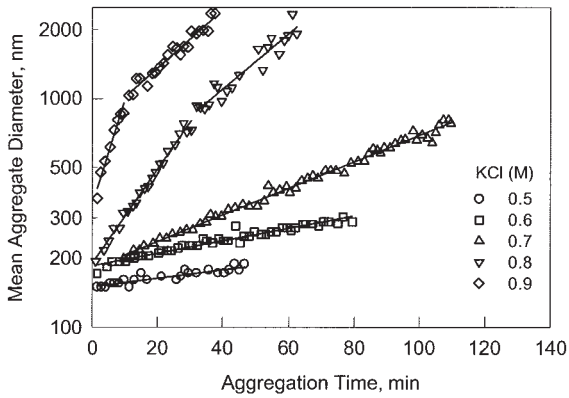

Figure 4 Semi-log plots for dynamic scaling of mean hydrodynamic diameter of γ-alumina aggregates in KCl solutions at pH 4.5, showing exponential growth kinetics and shift in slope at high salt concentrations (data from Beattie et al.[24]).

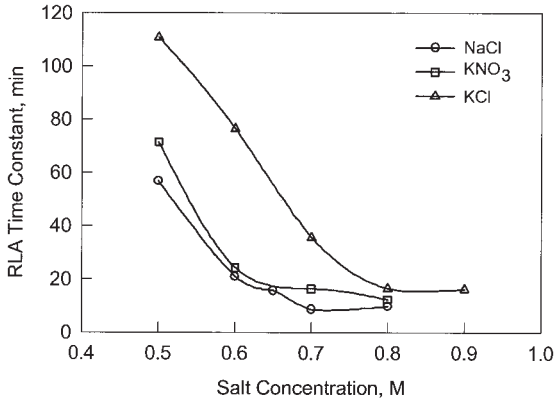

Figure 5 Variation of characteristic time constant of reaction-limited aggregation with salt concentration.

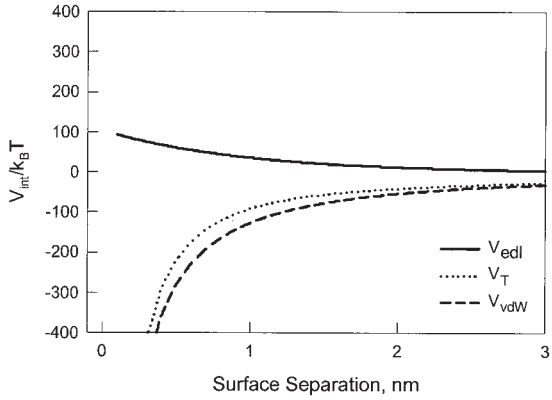

Figure 6 Interaction energy-surface separation diagram for γ-alumina particles computed from DLVO theory without including short-range structural repulsion, using Eq. 12 for V_{vdW} and Eq. 14 for V_{edl}.

Interaction energy between particles and hydration force parameters

The aggregation model has three adjustable parameters, hydration force constant (P_{hyd}), hydration decay length (λ_{hyd}) and proportionality constant in the collision kernel (K_{RLA}). Because of mutual compensation, the conventional approach to estimation of parameters together by minimizing an error function of a highly nonlinear model can lead to correlated and misleading values. We have, therefore, employed a systematic two-stage search strategy in order to ensure physically meaningful parameter values of the underlying phenomenon. In first stage, the interaction energy-surface separation diagram was utilized as a guide to determine hydration force parameters. In the second stage, the proportionality constant K_{RLA} was adjusted to match model simulation results with experimental data as closely as possible.

In order to map the interaction energy-surface separation diagram, it is necessary to have representative values for various inputs, such as Hamaker constant and particle surface potential. Ducker et al.[20] fitted forces between sapphire surfaces using a nonretarded Hamaker constant of 6.7×10^{-20} J. The same value was used in the Hamaker theory in Eq. 12 for computing van der Waals attraction between γ-alumina particles across water medium. The retardation factor was calculated from Eq. 13. The particle surface potential was assumed equal to zeta potential. The experimentally measured zeta potential of approximately 30 mV at pH 4.5[25] was employed for estimating the EDL repulsion, that is, $\psi_{0_k} = \psi_{0_l} = 30$ mV. The energy curves were calculated for interaction between spherical particles of $r_{0_k} = r_{0_l} = 60$ nm radius. As shown in Figure 6, at a KNO_3 concentration of 0.5 M the classical DLVO theory - in which total interaction energy is sum of van der Waals attraction and EDL repulsion energies only - predicts a strong attraction. It was, however, experimentally observed that aggregation did not take place until salt concentration is greater than 0.5 M. It is then reasonable to conclude that it is necessary to include a short-range repulsion force so as to preclude coagulation at this salt concentration. For this purpose, initial guesses of the two parameters in the structural repulsion equation were chosen from the ranges of their values that have been reported in literature. These values were next adjusted to ensure that the structural repulsion dominates the interaction.

After some trial and error, the values of P_{hyd} and λ_{hyd} were found to be approximately 1.9×10^7 N/m^2 and 0.6 nm, respectively, which are well within the ranges determined by surface force measurements[51]. Interestingly, the fitted hydration decay length of 0.6 nm is approximately equal to twice the diameter of water molecules, 0.275 nm. Using these parameter values, total interaction energy was computed as a sum of van der Waals attraction, EDL repulsion and structural repulsion. It will be observed from Figure 7 that the suspension is now predicted to be stable at 0.5 M KNO_3, as observed experimentally. However, it is close to the region where the suspension becomes unstable if double layer repulsion is suppressed. Simulation studies show that stability ratio W is quite sensitive to hydration force parameters. An increase in P_{hyd} results in an increase in W and enhanced suspension stability. Similarly, a reduction in P_{hyd} reduces W and increases the instability of suspension. On the other hand, λ_{hyd} has an opposite effect on W.

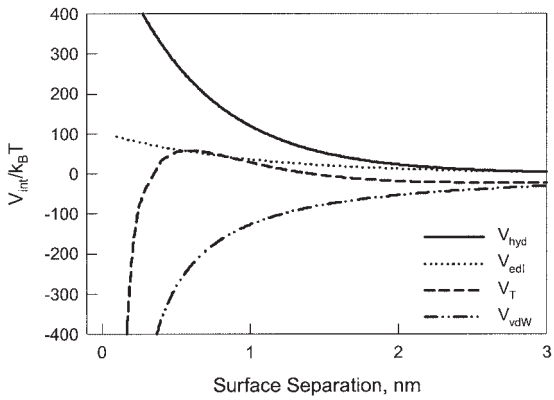

Figure 7 Interaction energy-surface separation diagram for γ-alumina particles computed from extended DLVO theory, including short-range structural repulsion, using Eq. 12 for V_{vdW}, Eq. 14 for V_{edl} and Eq. 17 for V_{hyd}.

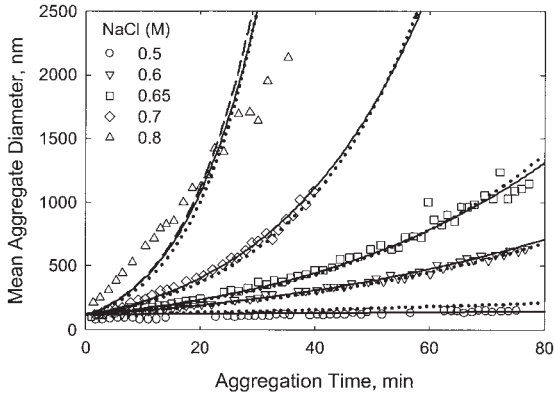

Figure 8 Simulated and experimental time evolution of mean hydrodynamic diameter of γ-alumina aggregates in NaCl solutions at pH 4.5 (solid lines - Eq. 9; dotted lines - Eq. 23; symbols - data from Waite et al.[25]).

Dashed lines are simulation results for 0.8 M NaCl including contribution from differential sedimentation, Eq. 21.

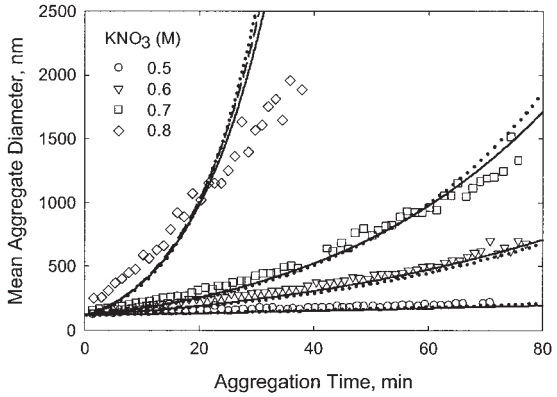

Figure 9 Simulated and experimental time evolution of mean hydrodynamic diameter of γ-alumina aggregates in KNO_3 solutions at pH 4.5 (solid lines - Eq. 9; dotted lines - Eq. 23; symbols - data from Waite et al.[25]).

Dashed lines are simulation results for 0.8 M KNO_3 including contribution from differential sedimentation, Eq. 21.

Model Validation

The discretized population balance equation in Eq. 2 was divided into 30 geometric sections, and the resulting 30 nonlinear ordinary differential equations were solved simultaneously by Gear's predictor-corrector numerical technique[57]. The stability ratio in Eq. 10 was evaluated by numerical integration using the Romberg algorithm[58], with $r_{0_k} = r_{0_l} = 60$ nm and $\psi_{0_k} = \psi_{0_l} = 30$ mV. During integration of population balance equations, the computed aggregate size distribution was tested at each time step for conservation of solid volume. The loss of total volume was less than 1% for the results presented here. The model was tested by comparing experimental data with model simulated time evolution of mass mean aggregate size, calculated in the following manner[14]

$$\bar{r} = \frac{\sum_i y_{N_i} r_{c_i}^4}{\sum_i y_{N_i} r_{c_i}^3} \tag{20}$$

where y_{Ni} is number fraction of aggregates belonging to section i and $\bar{r}$ is mass mean aggregate radius.

The simulated and experimental aggregate growth curves are shown in Figures 8, 9 and 10 for aggregation of γ-alumina in the presence of NaCl, KNO_3 and KCl, respectively. It will be seen that the computed growth curves are in reasonable agreement with the experimental data. The discrepancy between model predictions and experimental data at 0.8 M NaCl and KNO_3 is mainly because the aggregation process was assumed to follow RLA kinetics whereas it was actually in the transition region from RLA to DLA kinetics. That the process is in the transition regime is indicated by the linear growth behavior observed experimentally at 0.8 M in Figures 8 and 9. Similar results were reported by Weitz et al.[56] for aggregation of gold colloids. Since alumina is heavier than water, there is also a possibility of differential sedimentation influencing aggregate growth. In order to verify this, the collision kernel for aggregation at 0.8 M NaCl and KNO_3 was computed as a sum of contributions due to perikinetic aggregation (Eq. 9) and differential sedimentation. The collision frequency in the latter mechanism is given by[59]

$$\beta_{i,j}^{DS} = \frac{2\pi g}{9\mu}(r_{ci} + r_{cj})^2 |r_{ci}^2(\rho_i - \rho_l) - r_{cj}^2(\rho_j - \rho_l)| \tag{21}$$

where ρ_i and ρ_l are densities of aggregate and fluid, respectively, and g is acceleration due to gravity. The aggregate density ρ_i decreases as its size increases and it can be estimated using the following[60]

$$\rho_i = \rho_0 \left(\frac{r_{ci}}{r_0}\right)^{d_F - 3} \tag{22}$$

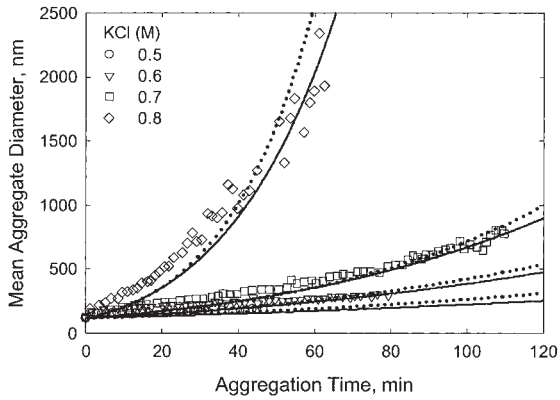

Figure 10 Simulated and experimental time evolution of mean hydrodynamic diameter of γ-alumina aggregates in KCl solutions at pH 4.5 (solid lines - Eq. 9; dotted lines - Eq. 23; symbols - data from Beattie et al.[24]).

Table 1. Computed Stability Ratio and Fitted RLA Kinetics Parameters

Figure No.	Reference	Salt	Salt Concentration (M)	Stability Ratio	K_{RLA} (m/s)	N_{11}
8	[25]	NaCl	0.5	9.49×10^6	7.0×10^{-3}	36
			0.6	1.78×10^6	5.0×10^{-3}	21
			0.65	0.88×10^6	3.5×10^{-3}	15
			0.7	0.46×10^6	3.4×10^{-3}	14
			0.8	0.15×10^6	2.2×10^{-3}	9
9	[25]	KNO_3	0.5	9.49×10^6	7.0×10^{-3}	36
			0.6	1.78×10^6	5.0×10^{-3}	21
			0.7	0.46×10^6	2.1×10^{-3}	9
			0.8	0.15×10^6	2.1×10^{-3}	9
10	[24]	KCl	0.5	9.49×10^6	7.0×10^{-3}	40
			0.6	1.78×10^6	2.5×10^{-3}	12
			0.7	0.46×10^6	1.0×10^{-3}	4.5
			0.8	0.15×10^6	1.0×10^{-3}	4.5

Note: The stability ratio was computed using Eq. 10, for $r_{0_k} = r_{0_l} = 60$ nm and $\psi_{0_k} = \psi_{0_l} = 30$ mV.

where ρ_0 is density of primary particles. This equation is strictly applicable for linear portion of the aggregate size-density curve. The simulation results obtained with this modification are shown as dashed lines in Figures 8 and 9 at 0.8 M NaCl and KNO_3, respectively. It can be observed that differential sedimentation does not contribute significantly to aggregate growth, presumably because aggregate density decreases as its size increases and aggregates in this study do not grow large enough for differential sedimentation to become significant. Consequently, transition regime is a more likely explanation for the process behavior under the stated conditions.

The deviation between computed and experimental results at 0.7 M KNO_3 in Figure 9 at longer aggregation times could be due to restructuring of aggregates. This is evident from the slight change in slope in Figure 3 for the same data after about 40 min of aggregation. Aggregate restructuring could also explain deviation between theory and experiment for the data at 0.8 M KCl in Figure 10. It can be seen from Figure 4 that the slope changes after about 30 min of aggregation. Our simulations of the aggregation process assume a constant fractal dimension of 2.1. It is, however, possible to obtain a better fit by employing a fractal dimension smaller than 2.1 at shorter aggregation times and a larger value at longer times. In fact, Selomulya et al.[61] developed an empirical expression for the evolution of aggregate fractal dimension with time, and fitted it to their experimental data for flocculation of latex particles in couette-flow. In view of the fact that the fitted parameters are specific to the experimental conditions employed, it was not possible to utilize the empirical expression of Selomulya et al.[61] in our analysis. Although there have been some studies on aggregate restructuring[62, 63], the phenomenon is not understood well enough to predict as to when and under what conditions it occurs.

The fitted proportionality constant in the collision kernel K_{RLA} and stability ratio, computed from Eq. 10, are included in Table 1. It is worth noting that computed stability ratios are comparable to experimentally determined values, although for a different material, polymer latex[64]. The reported stability ratios are within the range of $2.67 \times 10^5 - 4.41 \times 10^6$ for different solid and electrolyte concentrations. Note also the consistent trend in the variation of K_{RLA} and W with salt concentration in all cases analyzed. The results in Figures 8 – 10 strongly suggest that the collision kernel, proposed in Eq. 9, is able to represent the RLA kinetics quite accurately, at least for aggregation of alumina suspensions under the specified experimental conditions. Nevertheless, it is of some interest to carry out model simulation of these data with other prominent kernels in the literature. As mentioned earlier, Sandkuhler et al.[8] suggested that the following kernel by Odriozola et al.[9] is the most suitable among the kernels proposed for RLA

$$\beta_{i,j} = \frac{\beta_{Br}(n_{0_i}^{1/d_F} + n_{0_j}^{1/d_F})(n_{0_i}^{-1/d_F} + n_{0_j}^{-1/d_F})\, N_{11}(n_{0_i} n_{0_j})^{\lambda_O}}{4\{1 + W^{-1}[N_{11}(n_{0_i} n_{0_j})^{\lambda_O} - 1]\}} \tag{23}$$

This kernel contains two adjustable parameters N_{11}, which represents mean number of monomer collisions per encounter and λ_O, which is a numerical constant. Initially, we simulated aggregation of alumina suspensions employing this kernel with $N_{11} = 6.1$ and $\lambda_O = 0.4$, as reported by Lattuada et al.[64] for polystyrene latex, and the stability ratio values given in Table 1. The computed results turned out to be significantly different from the experimental data. Consequently, the two kernel parameters were adjusted for an acceptable fit. After some trial and error, λ_O was found to be 0.5, and N_{11} was found to decrease with increasing electrolyte concentration (see Table 1). The results obtained with the Odriozola et al.[9] kernel are shown as dotted lines in Figures 8 – 10. Although this kernel matches experimental data at lower salt concentrations well, it also fails to predict aggregation kinetics accurately at 0.8 M NaCl and KNO_3 in Figures 8 and 9, respectively. It should be noted here that the kernel in Eq. 9 employed by us involves only one adjustable parameter K_{RLA}, while the Odriozola et al. 9 kernel contains two parameters N_{11} and λ_0, which need to be adjusted depending on experimental conditions. As shown in Table 1, N_{11} varied with electrolyte concentration, while Lattuada et al.[64] found that λ_O changed with initial particle concentration.

Our kernel was next compared with a class of kernels employed previously for describing the RLA kinetics. There can be recast in a general form as follows[8]

$$\beta_{i,j} = \beta_{Br} B_{i,j} P_{i,j} \tag{24}$$

Table 2. Kernels Proposed in Literature for Reaction-Limited Aggregation Kinetics

Equation No.	$P_{i,j}$	Parameters	Reference
27	$[n_{0_i} - (n_{0_i}^{1/d_F} - 1)^{d_F}] \times [n_{0_j} - (n_{0_j}^{1/d_F} - 1)^{d_F}]$		[77]
28	$(\max(n_{0_i}, n_{0_j}))^{\lambda_B}$	$B_{i,j} = 1$ $\lambda_B = 1.0$	[1]
29	$(n_{0_i} n_{0_j})^{\lambda_P}$	$\lambda_P = 0.5$	[78]
30	$(n_{0_i}^{1/d_F} + n_{0_j}^{1/d_F})/2$		[8]
31	1		[7]

where

$$B_{i,j} = \frac{(n_{0_i}^{1/d_F} + n_{0_j}^{1/d_F})(n_{0_i}^{-1/d_F} + n_{0_j}^{-1/d_F})}{4} \tag{25}$$

and β_{Br} is the constant aggregation kernel or the collision frequency factor for two equal spheres in Brownian motion

$$\beta_{Br} = \frac{8k_BT}{3\mu} \tag{26}$$

The kernels differ mainly in the expression for $P_{i,j}$ (see Table 2). Simulation results obtained using different kernels are compared with experimental data for aggregation with 0.7 M NaCl in Figure 11. It was possible to match the experimental data with our kernel, Eq. 9 and that of Odriozola et al., Eq. 23 only, with stability ratio and kernel parameters given in Table 1, as shown previously in Figure 8. All the other kernels, given by Eq. 24 along with $P_{i,j}$ and parameters in Table 2, predict extremely slow aggregate growth at the same stability ratio, as seen in lines at the bottom and the insert in Figure 11. It was not possible to fit these kernels to experimental data even after adjusting the exponent values in them. The model predictions are, however, quite sensitive to parameters in these kernels.

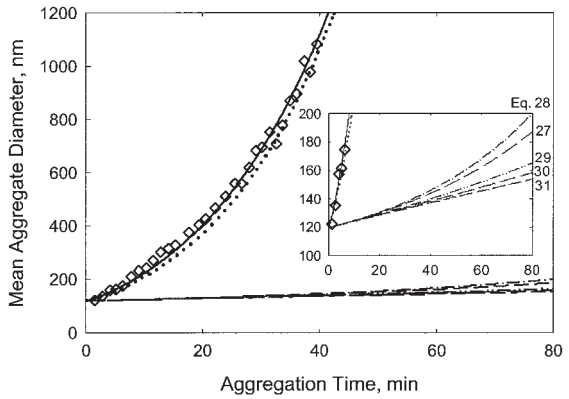

Figure 11 Time evolution of mean aggregate diameter predicted by various RLA kernels for aggregation of γ-alumina in 0.7 M NaCl solutions at pH 4.5 (solid lines - Eq. 9; dotted lines - Eq. 23; symbols - data from Waite et al.[25]).

The same plot on an expanded y-axis in insert shows the extremely slow kinetics predicted by kernels other than in Eqs. 9 and 23. See text for details of other kernels.

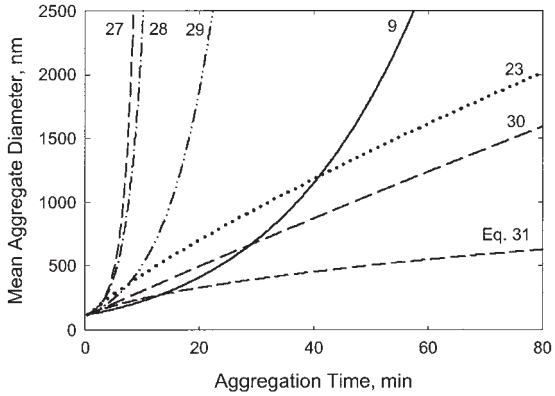

Figure 12 Time evolution of mean aggregate diameter predicted by various RLA kernels at a stability ratio of 10^4.

The general expression for kernels is given in Eq. 24 and expressions for $P_{i,j}$ in Table 2. Eq. 27 - Schmitt et al.[77]; Eq. 28 - Ball et al.[1]; Eq. 29 - product kernel[78]; Eq. 9 - kernel in present work, with $K_{RLA} = 10^{-4}$; Eq. 23 - Odriozola et al.[9] with $N_{11} = 2$ and $\lambda_O = 0.2$; Eq. 30 - sum kernel[8]; Eq. 31 - Smoluchowski kernel[7].

Since Figure 11 does not reveal enough information about the behavior of different kernels to permit a meaningful comparison among them, simulations were carried out at a lower stability ratio of 10^4 where noticeable aggregate growth occurs with all kernels, as shown in Figure 12. With $K_{RLA} = 10^{-4}$, our kernel, Eq. 9 predicts exponential growth, whereas the sum kernel, Eq. 30 leads to linear growth. The Smoluchowski kernel, Eq. 31 predicts power-law growth even at this high stability ratio. The rest predict exponential growth. The model predictions are quite sensitive to parameters in Odriozola et al. kernel, Eq. 23. It was already shown in Figures 8 –10 that exponential growth is predicted by this kernel with stability ratios and parameter values given in Table 1. However, it was also possible to obtain both linear as well as power-law growth by manipulating the parameters. For example, the model predicts power-law growth with $N_{11} = 2$ and $\lambda_O = 0.2$, as shown in Figure 12 (dotted line). Hence, only highly specialized numerical values of these parameters can lead to reaction-limited aggregation kinetics. On the other hand, our kernel, Eq. 9 predicts exponential growth at different stability ratios representative of RLA kinetics over a reasonably large range of numerical values of K_{RLA}.

Discussion

It is evident from the results shown in Figures 8-10 that the kernel employed in our model does represent the slow, exponential growth kinetics, typical of RLA, quite well. Unlike the kernels used previously for RLA, which are mostly empirical in nature, this kernel is based on theoretical proposition that the frequency of collisions between fractal aggregates depends on the total surface area of the interacting aggregates. The parameter K_{RLA} in the collision kernel is not completely arbitrary as it is apparently related to salt concentration. Even though solvent viscosity increases, the repulsive barrier between particles decreases with an increase in salt concentration and this is possibly the reason for decrease in K_{RLA} with salt content, as seen in Table 1. This is also an indirect indication that the

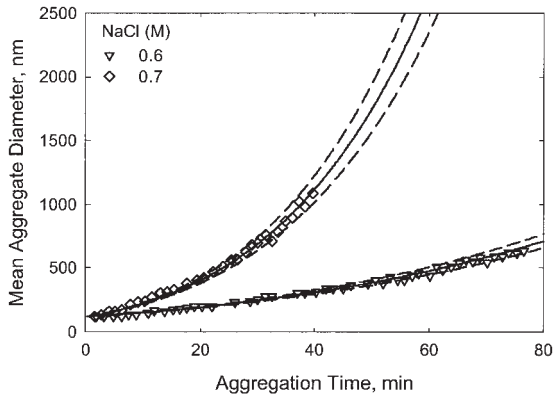

Figure 13 Sensitivity of model predictions to K_{RLA} using the present kernel, Eq. 9 for aggregation of γ-alumina in 0.6 M and 0.7 M NaCl solutions at pH 4.5.

Symbols are experimental data from Waite et al.[25]. Solid lines are model predictions using the best-fit K_{RLA} given in Table 1. Dashed lines are simulation results with ± 5% of best-fit K_{RLA}. Aggregate growth rate increases with K_{RLA}.

repulsive forces dictate the kinetics of reaction-limited aggregation, rather than diffusion of particles/aggregates. The sensitivity of aggregate growth to K_{RLA} is shown in Figure 13 for 0.6 M and 0.7 M NaCl concentrations. The solid lines are obtained with best-fit values given in Table 1 and the dashed lines on either side of the solid lines are with ± 5% of best-fit K_{RLA}. The mean aggregate diameter increases with K_{RLA}, and it is more sensitive to K_{RLA} at 0.7 M, presumably because the growth rate is higher at 0.7 M than at 0.6 M NaCl. Although this model can be used to predict aggregation kinetics that follows exponential growth, it is necessary to adjust K_{RLA} to match experimental data at different electrolyte concentrations. Experimental studies on RLA are relatively scarce as compared to DLA. One could possibly derive a useful expression for K_{RLA} as a function of experimental conditions, especially electrolyte concentration, if more data on RLA kinetics are available.

The hydration force parameters are not only physically meaningful, but are also within the range determined by surface force measurements. Moreover, their values are decoupled from the proportionality constant in the collision kernel K_{RLA}. The stability ratios computed from force parameters are reasonably close to experimentally determined values[64]. Unfortunately, with the current status of theories of structural forces, it is not possible to predict *a priori* under what conditions of pH and electrolyte concentration the short-range structural forces become operative and or predominant. It is well known that pH, electrolyte type and its concentration have a profound effect on coagulation and flocculation. For example, in case of metal or ceramic oxides, rate of aggregation increases as pH approaches the isoelectric point (IEP) of the oxide and decreases as pH moves away from IEP. Tjipangandjara et al.[65] found that the percent of alumina settled is maximum at pH 9, the IEP of alumina. This is mainly because aggregate mean size is also maximum at the IEP, as demonstrated by Rattanakawin and Hogg[66]. Similarly, aggregate growth rate of hematite suspensions increased with pH, became maximum at the IEP of hematite and then decreased at higher pH[67, 68]. The main reason for the dependence of aggregation kinetics on pH is due to its effect on surface potential of oxide materials. Both alumina and hematite are positively charged below the IEP and negatively charged at higher pH[69]. The magnitude of electrical double layer repulsion depends strongly on surface potential and essentially determines the kinetics of aggregation and aggregate fractal dimension. For example, Herrington and Midmore[70] found that the fractal dimension of kaolinite flocs decreased sharply from 2.8 at pH 3 to about 1.8 at pH 4 in pure water and from 2.9 at pH 3.5 to about 1.8 at pH 4.5 in 1 mM KCl solution. Similar results were reported for bentonite flocs[71]. The aggregate fractal dimension depends not only on pH but also on other variables, such as electrolyte concentration[14, 72], initial particle concentration[72] and temperature[73, 74]. Since a phenomenological model to predict fractal dimension is not available, we are obliged to treat it as an experimentally measured model input, as have other researchers also.

Finally, even though it is possible to predict reaction-limited aggregation kinetics in the presence of different electrolytes reasonably well, this model does not explicitly account for the influence of type or nature of co- or counter-ions. In principle, however, the model can be extended by incorporating a surface complexation or site-binding model of Leckie and coworkers[75,76] which can predict the surface or solid-liquid interface potential as a function of the nature of counterions.

Conclusions

Reaction-limited aggregation follows slow, exponential growth kinetics. This is mainly because efficiency of particle or aggregate collisions is very low, which is due to the presence of repulsive electrical double layer and short-range structural or hydration forces. We have presented a population balance model for reaction-limited aggregation of colloidal suspensions, and tested it with experimental data for aggregation of alumina suspensions in the presence of different electrolytes. Instead of employing an empirical collision kernel, a theoretical kernel, derived from arguments of Ball et al.[1] and based on total surface area of interacting aggregates, is proposed to model the slow, exponential aggregate growth kinetics. This kernel represents experimental data more accurately than the kernels previously suggested in the literature.

Another feature of this model is that it incorporates a theoretical model for predicting the collision efficiency factor, instead of using it as a fitting parameter. The collision efficiency factor was computed as a function of surface forces, namely, van der Waals attraction, electrical double layer repulsion and short-range structural repulsion. This allows us to take into account the effect of important process variables, such as solution pH and electrolyte concentration on aggregation, which was not possible with previous population balance models.

Acknowledgments

This work was supported by the National Science Foundation (NSF Grants # INT-96-05197 and INT-01-17622) and the NSF Industry/University Cooperative Research Center (IUCRC) for Advanced Studies in Novel Surfactants at Columbia University (NSF Grant # EEC-98-04618). The authors thank the management of Tata Research Development and Design Centre for the permission to publish this article. VR thanks Prof.E.C.Subbarao, Prof.Mathai Joseph and Dr.Pradip for their advice and encouragement.

Notation

A = Hamaker constant of solid particles across a solvent, J
b_i = upper boundary volume of section i, m^3
C_L = aggregate structure prefactor, dimensionless
D = hydrodynamic correction factor, dimensionless
d_F = fractal dimension of flocs, dimensionless
e = elementary charge, C
F_{hyd} = hydration/structural repulsion force between two flat surfaces, N/m^2
f_R = retardation correction function, dimensionless
g = acceleration due to gravity, m/sec^2
g_R = parameter in the retardation correction function, dimensionless
h_0 = distance of closest approach between particle surfaces, m
$\bar{h}_0$ = normalized distance of closest approach, dimensionless
h_w = distance over which two clusters touch each other, m
I = ionic strength of solution, mol/m^3
K_{RLA} = proportionality constant in RLA kernel, m/s
k_B = Boltzmann constant, J/K
M = mass of an aggregate, kg
max = maximum number of sections considered in population balance
n = number concentration of particles or aggregates, m^{-3}
n_0 = number of primary particles in an aggregate, dimensionless
N_{Av} = Avagadro's number, mol^{-1}
N_i = number concentration of particles or aggregates in section i, m^{-3}
N_{11} = mean number of monomer collisions per encounter, dimensionless
P_{hyd} = hydration/structural force constant, N/m^2
r_{c_i} = collision radius of an aggregate belonging to section i, m
r_0 = mean radius of primary particles, m
r_n = characteristic size of an aggregate, m
$\bar{r}$ = mass mean radius of an aggregate, m
r_1, r_2 = radii of two spherical particles 1 and 2, m
s = particles' center-to-center separation distance, m
t = aggregation time, sec
T = suspension temperature, K
u = volume of a particle or an aggregate, m^3
v = volume of a particle or an aggregate, m^3
V_f = volume of phase-space in which two clusters are in bondable contact, m^3
V_{hyd} = hydration/structural repulsion energy between two particles, J
V_i = characteristic volume of an aggregate in section i, m^3
V_{int} = interaction energy between two primary particles, J
V_{vdW} = van der Waals attraction energy between two primary particles, J
V_{edl} = electrical double layer repulsion energy between two primary particles, J
V_T = total interaction energy between two primary particles, J
W = stability ratio, dimensionless
y_{N_i} = number fraction of aggregates belonging to section i, dimensionless
z_c = counterion valence, dimensionless

Greek letters

α = collision efficiency factor, dimensionless
β = collision frequency factor, m^3/s
β_i^{DS} = collision frequency due to differential sedimentation, m^3/s
β_{Br} = collision frequency factor for two equal spheres in Brownian motion, m^3/s
ε_0 = dielectric constant of free space C/m-V
ε_r = dielectric constant of water or solvent, C/m-V
κ = Debye-Huckel parameter, m^{-1}
λ_O = numerical constant in Odriozola kernel, dimensionless
λ_{hyd} = hydration decay length, m
λ_R = characteristic wave length of interaction, m
μ = dynamic viscosity of the suspending fluid, kg/m-sec
ρ_0 = density of primary particles, kg/m^3
ρ_i = density of an aggregate in section i, kg/m^3
ρ_l = fluid density, kg/m^3
ψ_0 = particle surface potential, V
τ_{RLA} = characteristic time constant of RLA, min

Literature Cited

1. Ball RC, Weitz DA, Witten TA, Leyvraz F. Universal kinetics in reaction-limited aggregation. *Phys Rev Lett*. 1987;58:274-277.
2. Dobias B. *Coagulation and Flocculation: Theory and Applications*, New York: Marcel Dekker, Inc., 1993.
3. Pugh RJ, Bergstrom L. *Surface and Colloid Chemistry in Advanced Ceramics Processing*. New York: Marcel Dekker, Inc., 1994.
4. Somasundaran P, Das KK, Yu X. Selective flocculation. *Curr Opinion Colloid Interface Sci*. 1996;1:530-534.
5. Jackson GA, Burd AB. Aggregation in the marine environment. *Env Sci Tech*. 1998;32:2805-2814.
6. Lin MY, Lindsay HM, Weitz DA, Ball RC, Klein R, Meakin P. Universality in colloid aggregation. *Nature*. 1989;339:360-362.
7. Smoluchowski, Mv. Versuch einer mathematischen theorie der koagulationskinetik kolloider losungen. *Zietschrift fur Physikalische Chemie*. 1917;92:129-168.
8. Sandkuhler P, Sefcik J, Lattuada M, Wu H, Morbidelli M. Modeling structure effects on aggregation kinetics in colloidal dispersions. *AIChE J*. 2003;49:1542-1555.
9. Odriozola G, Moncho-Jorda A, Schmitt A, Callejas-Fernandez J, Martinez-Garcia R, Hidalgo-Alvarez R. A probabilistic aggregation kernel for the computer-simulated transition from DLCA to RLCA. *Europhys Lett*. 2001; 53:797-803.
10. van Dongen PG, Ernst MH. Dynamic scaling in the kinetics of clustering. *Phys Rev Lett*. 1985;54:1396-1399.
11. Martin JE, Wilcoxon JP, Schaefer D, Odinek J. Fast aggregation of colloidal silica. *Phys Rev A*. 1990;41:4379-4391.
12. von Schulthess GK, Benedek GB, De Blois RW. Measurement of the cluster size distributions for high functionality antigens crosslinked by antibody. *Macromolecules*. 1980;13:939-945.
13. Weitz DA, Lin MY. Dynamic scaling of cluster-mass distributions in kinetic colloid aggregation. *Phys Rev Lett*. 1986;57:2037-2040.
14. Amal R, Coury JR, Raper JA, Walsh WP, Waite TD. Structure and kinetics of aggregating colloidal hematite. *Colloids Surfaces A*. 1990; 46:1-19.
15. Runkana V, Somasundaran P, Kapur PC. Mathematical modeling of polymer-induced flocculation by charge neutralization. *J Colloid Interface Sci*. 2004;270:347-358.
16. Derjaguin BV, Landau LD. A theory of the stability of strongly charged lyophobic sols and of the adhesion of strongly charged particles in solutions of electrolytes. *Acta Physiochim. USSR*. 1941;14: 633-662.
17. Verwey EJW, Overbeek JThG. *Theory of the Stability of Lyophilic Colloids*. Amsterdam: Elsevier, 1948.
18. Pashley RM. DLVO and hydration forces between mica surfaces in Li^{+1}, Na^{+1}, K^{+1}, and Cs^{+1} electrolyte solutions in the range 1-100 nm. *J Colloid Interface Sci*. 1981;83:531-546.
19. Pashley RM, Israelachvili JN. DLVO and hydration forces between mica surfaces in Mg^{+2}, Ca^{+2}, Sr^{+2}, and Ba^{+2} chloride solutions. *J Colloid Interface Sci*. 1984;97:446-455.
20. Ducker WA, Xu Z, Clarke DR, Israelachvili JN. Forces between alumina surfaces in salt solutions: non-DLVO forces and the implications for colloidal processing. *J Am Ceram Soc*. 1994; 77:437-443.
21. Karaman ME, Pashley RM, Waite TD, Hatch SJ, Bustamante H. A comparison of the interaction forces between model alumina surfaces and their colloidal properties. *Colloids Surfaces A*. 1997;129-130:239-255.
22. Velamakanni BV, Chang JC, Lange FF, Pearson DS. New method for efficient colloidal particle packing via modulation of repulsive lubricating hydration forces. *Langmuir*. 1990;6:1323-1325.
23. Molina-Bolivar JA, Ortega-Vinuesa JL. How proteins stabilize colloidal particles by means of hydration forces. *Langmuir*. 1999;15:2644-2653.
24. Beattie JK, Cleaver JK, Waite TD. Anomalous aggregation behavior of aluminium oxyhydroxides. *Colloids Surfaces A*. 1996;111:131-138.
25. Waite TD, Cleaver JK, Beattie JK. Aggregation kinetics and fractal structure of γ-alumina assemblages. *J Colloid Interface Sci*. 2001;241: 333-339.
26. van Bruggen MPB, Donker M, Lekkerkerker HNW, Hughes TL. Anomalous stability of aqueous boehmite dispersions induced by hydrolyzed aluminium poly-cations. *Colloids Surfaces A*. 1999;150: 115-128.
27. Ramkrishna D. *Population Balances: Theory and Applications to*

Particulate Systems in Engineering. New York: Academic Press, 2000.
28. Vanni M. Approximate population balance equations for aggregation - breakage processes. *J Colloid Interface Sci*. 2000;221:143-160.
29. Hounslow MJ, Ryall RL, Marshall VR. A discretized population balance for nucleation, growth, and aggregation. *AIChE J*. 1988;34: 1821-1832.
30. Spicer PT, Pratsinis SE. Coagulation and fragmentation: universal steady-state particle-size distribution. *AIChE J*. 1996;42:1612-1620.
31. Flesch JC, Spicer PT, Pratsinis SE. Laminar and turbulent shear-induced flocculation of fractal aggregates. *AIChE J*. 1999;45:1114-1124.
32. de Boer GBJ. *Coagulation in Stirred Tanks*. PhD Thesis. Eindhoven University of Technology. The Netherlands. 1987.
33. Ducoste JJ. A two-scale PBM for modeling turbulent flocculation in water treatment processes. *Chem Eng Sci*. 2002;57:2157-2168.
34. Firth BA, Hunter RJ. Flow properties of coagulated colloidal suspensions I. energy dissipation in the flow units. *J Colloid Interface Sci*. 1976;57:248-256.
35. Kusters KA, Wijers JG, Thoenes D. Aggregation kinetics of small particles in agitated vessels. *Chem Eng Sci*. 1997;52:107-121.
36. Fuchs N. Ueber die stabilitat und aufladung der aerosole. Zeitschrift fur Physik. 1934;89:736-743.
37. Derjaguin BV, Muller VM. Slow coagulation of hydrophobic colloids. *Dokl Akad Nauk SSSR*. 1967;176:738-741.
38. McGown DN, Parfitt GD. Improved theoretical calculation of the stability ratio for colloidal systems. *J Phys Chem*. 1967;71:449-450.
39. Spielman LA. Viscous interactions in Brownian coagulation. *J Colloid Interface Sci*. 1970;33:562-571.
40. Honig EP, Roebersen GJ, Wiersema PH. Effect of hydrodynamic interaction on the coagulation rate of hydrophobic colloids. *J Colloid Interface Sci*. 1971;36:97-109.
41. Hamaker HC. The London-van der Waals attraction between spherical particles. *Physica*. 1937;IV:1058-1072.
42. Lifshitz EM. The theory of molecular attractive forces between solids. *Soviet Physics JETP*. 1956;2:73-83.
43. Bowen WR, Jenner F. The calculation of dispersion forces for engineering applications. *Adv Colloid Interface Sci*. 1995;56:201-243.
44. Israelachvili JN. *Intermolecular and Surface Forces*. 2nd ed. New York: Academic Press, 1991.
45. Gregory J. Approximate expressions for retarded van der Waals interaction. *J Colloid Interface Sci*. 1981;83:138-145.
46. Hogg R, Healy TW, Fuerstenau DW. Mutual coagulation of colloidal dispersions. *Trans Faraday Soc*. 1966;62:1638-1651.
47. Bell GM, Levine S, McCartney LN. Approximate methods of determining the double-layer free energy of interaction between two charged colloidal spheres. *J Colloid Interface Sci*. 1970;33:335-359.
48. Sader JE, Carnie SL, Chan DYC. Accurate analytic formulas for the double-layer interaction between spheres. *J Colloid Interface Sci*. 1995;171:46-54.
49. Johnson SB, Franks GV, Scales PJ, Boger DV, Healy TW. Surface chemistry - rheology relationships in concentrated mineral suspensions. *Int J Miner Process*. 2000;58:267-304.
50. Manciu M, Ruckenstein E. Role of the hydration force in the stability of colloids at high ionic strengths. *Langmuir*. 2001;17:7061-7070.
51. Thompson DW, Collins IR. Electrolyte-induced aggregation of gold particles on solid surfaces. *J Colloid Interface Sci*. 1994;163:347-354.
52. Derjaguin BV. Friction and adhesion. IV. The theory of adhesion of small particles. *Kolloid-Z*. 1934;69:155-164.
53. Broide ML, Cohen RJ. Experimental evidence of dynamic scaling in colloidal aggregation. *Phys Rev Lett*. 1990;64:2026-2029.
54. Lin MY, Lindsay HM, Weitz DA, Ball RC, Klein R, Meakin P. Universal reaction-limited colloid aggregation. *Phys Rev A*. 1990;41: 2005-2020.
55. Schaefer DW, Martin JE, Wiltzius P, Cannell DS. Fractal geometry of colloidal aggregates. *Phys Rev Lett*. 1984;52:2371-2374.
56. Weitz DA, Huang JS, Lin MY, Sung J. Limits of the fractal dimension for irreversible kinetic aggregation of gold colloids. *Phys Rev Lett*. 1985;54:1416-1419.
57. Gear CW. *Numerical Initial Value Problems in Ordinary Differential Equations*. Englewood Cliffs, NJ, USA: Prentice-Hall, 1971.
58. Press WH, Teukolsky SA, Vetterling WT, Flannery BP. *Numerical Recipes in FORTRAN: the Art of Scientific Computing*. 2nd ed. New York: Cambridge University Press, 1992.
59. Camp TR, Stein PC. Velocity gradients and internal work in fluid motion. *J Boston, Soc Civ Eng*. 1943;30,219-237.
60. Jiang Q, Logan BE. Fractal dimensions of aggregates determined from steady-state size distributions. *Env Sci Tech*. 1991;25,2031-2038.
61. Selomulya C, Bushell G, Amal R, Waite TD. Understanding the role of restructuring in flocculation: The application of a population balance model. *Chem Eng Sci*. 2003;58:327-338.
62. Aubert C, Cannell DS. Restructuring of colloidal silica aggregates. *Phys Rev Lett*. 1986;56:738-741.
63. Selomulya C, Amal R, Bushell G, Waite TD. Evidence of shear rate dependence on restructuring and breakup of latex aggregates. *J Colloid Interface Sci*. 2001;236:67-77.
64. Lattuada M, Sandkuhler P, Wu H, Sefcik J, Morbidelli M. Aggregation kinetics of polymer colloids in reaction limited regime: experiments and simulations. *Adv Colloid Interface Sci*. 2003;103:33-56.
65. Tjipangandjara K, Huang YB, Somasundaran P, Turro NJ. Correlation of alumina flocculation with adsorbed poly(acrylic acid) conformation. *Colloids Surfaces A*, 1990;44:229-236.
66. Rattanakawin C, Hogg R. Aggregate size distributions in flocculation. *Colloids Surfaces A*. 2001;177:87-98.
67. Schudel M, Behrens SH, Holthoff H, Kretzschmar R, Borkovec M. Absolute aggregate rate constants of hematite particles in aqueous suspensions: a comparison of two different surface morphologies. *J Colloid Interface Sci*. 1997;196:241-253.
68. Gardner KH, Theis TL, Young TC. Colloid aggregation: numerical solution and measurements. *Colloids Surfaces A*. 1998;141:237-252.
69. Hunter RJ. *Zeta Potential in Colloid Science: Principles and Applications*. New York: Academic Press, 1981.
70. Herrington TM, Midmore BR. Investigation of scaling effects in the aggregation of dilute kaolinite suspensions by quasi-elastic light scattering. *Colloids Surfaces A*. 1993;70:199-202.
71. Axford SDT, Herrington TM. Determination of aggregate structures by combined light-scattering and rheological studies. *J Chem Soc., Faraday Trans*. 1994;90:2085-2093.
72. Burns JL, Yan Yd, Jameson GJ, Biggs S. A light scattering study of the fractal aggregation behavior of a model colloidal system. Langmuir. 1997;13:6413-6420.
73. Tang P, Colflesh DE, Chu B. Temperature effect on fractal structure of silica aggregates. *J Colloid Interface Sci.* 1988;126:304-313.
74. Amal R, Raper JA, Waite TD. Fractal structure of hematite aggregates. J. Colloid Interface Sci. 1990; 140,158-168.
75. Davis JA, James RO, Leckie JO. Surface ionization and complexation at the oxide/water interface. I. computation of electrical double layer properties in simple electrolytes. J. Colloid Interface Sci. 1978;63:480-499.
76. Davis JA, Leckie JO. Surface ionization and complexation at the oxide/water interface. II. surface properties of amorphous iron oxyhydroxide and adsorption of metal ions. J. Colloid Interface Sci. 1978; 67:90-107.
77. Schmitt A, Odriozola G, Moncho-Jorda A, Callejas-Fernandez J, Martinez-Garcia R, Hidalgo-Alvarez R. Multiple contact kernel for diffusionlike aggregation. Phys. Rev. E, 2000;62:8335-8343.
78. Family F, Meakin P, Vicsek T. Cluster size distribution in chemically controlled cluster-cluster aggregation. J. Chem. Phys. 1985;83,4144-4150.

Manuscript received Jan. 4, 2004, and revision received Aug. 1, 2004.